Singh et al. 2018. *Int. J. Vehicle Structures & Systems*, 10(4), 231-245
ISSN: 0975-3060 (Print), 0975-3540 (Online)
doi: 10.4273/ijvss.10.4.02

International Journal of Vehicle Structures & Systems
Available online at www.maftree.org/eja

Dynamic Analysis of Linke Hofmann Busch Coach and Determination of its Sensitive Design Parameters Considering Suspended Equipments

S.D. Singh[a], Rakesh Mathur[b] and R.K. Srivastava[c]

[a]*Dept. of Applied Mechanics, MNNIT, Allahabad, India*
Mechanical Dept. of North Central Railway, Indian Railway, Allahabad, India
Corresponding Author, Email: sds_me@rediffmail.com
[b]*Dept. of Applied Mechanics, MNNIT, Allahabad, India*
Email: rm30@rediffmail.com
[c]*Dept. of Mech. Engg., MNNIT, Allahabad, India*
Email: rks@mnnit.ac.in

ABSTRACT:

This study aims at dynamic behaviour of a Linke Hofmann Busch coach and its sensitive parameters against track irregularities considering various suspended equipment. The randomly distributed track irregularities characterized in terms of Indian Rail Road PSD standard are considered main source of excitation that produces undesired vibrations. The coach body and bogie frame subjected to 4 degree of freedom motions (bounce, lateral, roll and pitch) are modelled using finite element methodology where system matrices such as mass, stiffness and damping matrices are obtained for eigenvalue solution. Using modal parameters obtained as above and PSD of track irregularities, both vertical and lateral mean square acceleration responses (MSAR) are determined at various points of concern on coach body. It is observed that the vertical peak responses occur in low frequency range (0-10 Hz) which is caused by long wavelength irregularities of track that causes discomfort. It is also observed that constant peak lateral responses occur at still lower frequency as compared to vertical response which again causes discomfort to vehicle riders. This concludes that there is a further scope of improvement in comfort level with minor adjustments of suspended equipment of a LHB coach. A sensitivity analysis based on the partial derivatives against FRF displacement is conducted and most sensitive design parameters are obtained for optimization to improve ride comfort. It is suggested that if the mass of bio toilet tanks and relative position of battery box + transformer unit i.e. most sensitive parameters of suspended equipment are changed then the ride comfort can be improved.

KEYWORDS:

Linke Hofmann Busch coach; Suspended equipments; Power spectral density; Dynamic responses; Finite elements

CITATION:

S.D. Singh, R. Mathur and R.K. Srivastava. 2018. Dynamic Analysis of Linke Hofmann Busch Coach and Determination of its Sensitive Design Parameters Considering Suspended Equipments, *Int. J. Vehicle Structures & Systems*, 10(4), 231-245. doi:10.4273/ijvss.10.4.02.

1. Introduction

Rail wheel running on irregular track receives an excitation and produces undesired vibrations. These are caused due to track surface irregularities, wheel out of roundness (OOR), train track interaction, variation in track sleepers spacing and its stiffness, impact load caused by traction etc. From all these factors, rail surface irregularities are the major sources of excitation. Train track interaction force generates vibration that leads to track deterioration producing uneven rail track geometry which causes long and short wavelength (λ) vertical and lateral irregularities. Vertical irregularities of rail surface are one of the essential sources of vibration and responsible both for vertical and lateral vibration in the high speed train system [1]. Rigid body of vehicles such as car body, bolsters, bogie frames and wheel axles execute different angular motions i.e. roll, pitch and yaw influencing the dynamics of rail vehicle system [2]. Running vehicle on track is always accompanied with coupled vertical and lateral motions. There has been extensive work done by many researchers on the vertical and lateral dynamics of rail vehicle in order to study these motions separately. While run on irregular track, each wheel of vehicle is considered a source of an excitation through which vibrations are transmitted to the car body thereby giving rise to undesired vibrations. It was described that dynamic effects or vibration pronounced more in the train-track system when train speed and the axle load increase [3]. These excessive vibrations are further amplified by the surface irregularities which are harmful and undesirable [4-5].

Modelling of rail vehicle under track irregularities has been primary requirement to study the ride comfort and dynamic behaviour and hence many researchers have studied dynamic behaviour of vehicle. Researchers have described 4 type sources of excitation namely quasi static, parametric stiffness variation, dynamic excitation caused by the wheel and track irregularities and excitation generated by high speed train compared to Rayleigh surface waves in the ground [5]. Irregularities

of track surface are assumed to be random profile follow Gaussian distribution and exciting force input between wheel and rail is determined from its auto and cross correlation functions. Cheli and Corradi [6] analysed the excitation mechanism and induced vibrations on rail car body due to track unevenness and responses determined in rigid and flexible mode. Result concluded that the flexible mode excitation has effective role on acceleration.

Yalcin et al [4] discussed ballasted and slab tracks under different operating speeds and concluded that at low frequency range tracks behave like rigid spring and have no remarkable effect on vehicle dynamics. Modelling and simulation of rail vehicles have been accomplished either in time domain or frequency domain analysis with regard to ride comfort. Zadeh et al [7] performed response modelling of half rail bogie on irregular track both in time and frequency domains and result observed that PSD of rail track decreases with increasing speed parameter. The following paragraph includes some of studies to bring out research gap and formulate the objective of this paper. Zhai and Cai [8] presented modelling and simulation of rail vehicle and track in time domain using D's Alembert principle considering nonlinear hertz wheel - rail contact model and concluded that contact irregularities are the main source of dynamic disturbances. Broussinos and Kabe [9] presented matrix formulation for multimode Gaussian random response analysis of vehicle in frequency domain by taking excitations in terms of auto and cross power spectral density functions and concluded that the responses become consistent with the time domain when cross-spectrum of input forces are taken. Similarly, Gangadharan et al [10] presented an experimental and analytical method to evaluate ride index and ride comfort of suburban rail vehicle using FE model. Results concluded that extreme end of coach body has higher vibration level. The lateral acceleration remains constant along the length of the coach body.

Modelling and simulation of Indian Railway Rajdhani and General sleeper coach having 37 DOF coupled vertical, lateral, roll, pitch and yaw motions was carried out in frequency domain using Lagrangian method and result compared with ISO 2631 comfort criteria that suggest scope for improvement in the design of rail vehicle in low frequency range 1-10 Hz [11]. Response of a rail vehicle under 6 DOF was analysed in frequency domain for variable speed using Lagrangian equation and result concluded that level of passenger comfort depends on the level of acceleration response [4]. Gangadharan et al [12] studied vertical and lateral response analysis of FE model of rigid suburban coach in frequency domain under 3DOF motions (bounce, pitch and roll) and found that rigid body model underestimates the response and FE model predicts response closer to measured value. Yunesian et al [13], described time domain spectral analysis with PSD in frequency domain for high speed train. Genetic algorithms an optimization technique was applied for optimal design of vehicle's parameters at variable speed. Jinhui Xu et al [14] studied frequency response of vehicle-track vertical coupled system both in time and frequency domain and suggested that vertical vibration increases with vehicle speed. Razvan [15] applied random vibration simulation method for vehicle analysis where mode shapes, Eigen frequencies, Power Spectral Density (PSD) profiles and input matrix of cross spectral powers were determined. Mădălina Dumitriu [16] modelled rail car body as an Euler Bernoulli beam and root mean square acceleration was determined. Results revealed that vertical comfort index decreases at centre and increases on towards ends.

Sun et al [17] described vertical rigid and flexible high speed rail vehicle model for single suspended equipment location and ride quality is analysed using co-variance methods. The suspended device stiffness at centre of car body influences the vertical ride and bigger device mass is better for ride quality. Bao et al [18] described a suspended monorail transit system for bridge and vehicle response analyses considering train formation, track irregularity and rubber tire stiffness. The Guyan condensation method was used to reduce the DOF and tire stiffness of mono rail observed to be most sensitive to response. On the basis of various rail vehicle response analyses, ride quality and ride comfort is determined from root mean square acceleration and investigated in applicable human sensation non-audible frequency range where its magnitudes need to be remained minimum in low frequency range i.e. 0-20 Hz [19]. Apart from the modelling of rail vehicle, various researchers have also focused their research attention on parametric sensitivity analysis to find out its effects on response level. To [20] described the dynamic behaviour of rail structure's model sensitivity analysis by partial derivatives of eigenvalues and eigenvectors with respect to stiffness [K] and mass [M] matrices and optimum design was obtained.

Sharma [2] studied influence of rail vehicle parameters on ride behaviour by varying - 20% to + 20% of original values and suggested lower values of suspension vertical stiffness with higher wheel base for all frequency range except 3-4.25 Hz. Sharma [1] conducted a sensitivity analysis of Indian Railway Rajdhani coach to observe effects of car body mass, roll, pitch, yaw, MI, spring's stiffness, damping coefficient and wheel base on response and indicated that mass and pitch MI are the most sensitive parameters. Bhattacharjee et al [21] analysed correlation between derailment safety and ride comfort of Indian Railway vehicle and suggested ride comfort is more sensitive to secondary suspension. Rail vehicle is modelled by considering either of vertical, longitudinal, lateral, rolling, yawing motions or its coupled motions. Most of such work has been carried out by taking separate consideration of vertical and lateral including pitch, yaw and roll motions. In [17], response of rail vehicle was analysed for single suspended equipment close to centre mass of car body and its influence on ride behaviour. Similarly, suspended monorail transit system was analysed by the literature [18]. In practice, there are numbers of suspended equipments underneath coach.

The relative spatial distances, masses and suspension stiffness of such suspended equipment can have substantial effect on response level and affect ride comfort. In view of that, present paper addresses to the model of German designed Linke Hofmann Busch

(LHB) coach of Indian Railway consisting various suspended equipment and subjected to 4DOF coupled motions are considered for modelling and response analysis. Further, a finite element (FE) technique is used and the model is reduced for bounce and lateral motions using Guyan reduction technique [22]. Also, the coach is modelled for sensitive parameters through mathematical approach of partial derivative against FRF displacement. The mathematical formulation for displacement response PSD is derived from the earlier work of [11, 13, 23]. The acceleration response PSD or mean square acceleration response (MSAR) is calculated as,

$$\text{MSAR} = (\text{frequency})^4 \times \text{Displacement response PSD}$$

The proposed method in this paper is applied to a typical model of rail vehicle while running on irregular track and MSAR are determined in low frequency range.

2. Rail track irregularities and modelling of rail vehicle

2.1. Rail track irregularities

No track is aligned and laid down perfectly. Hence there will always be some deviation in its settlement causing deterioration (+/-50 mm vertical and +/-10 mm lateral deviations) by which oscillations or vibrations takes place [3]. This track deterioration produces uneven track profile which causes long wavelength (λ) irregularities (1-100 m) giving low frequency < 20 Hz excitation bringing about discomfort to travelling passengers whereas short wavelength (λ) irregularities (3-300 mm) causes high frequencies > 150 Hz excitation as noise discomfort to the travelling passengers and resident nearby railway lines [24]. European standard EN 13848 has also classified track sections based on long wavelengths (λ) irregularities: D_1 (3-35 m), D_2 (25-70 m) and D_3 (70-150 m) [25]. Long and short pitch vertical irregularities of track are shown in Fig. 1 [26-27].

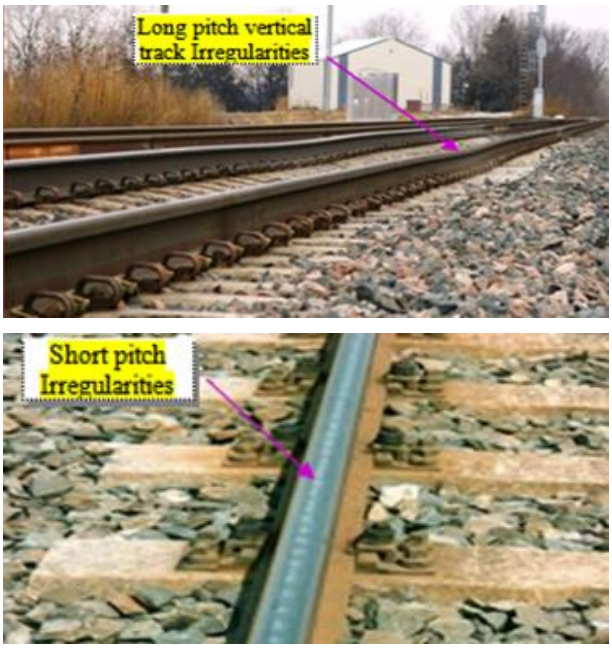

Fig. 1: Typical rail track long and short pitch irregularities

2.2. PSD of track irregularities

The variation in the vertical or lateral profile on either surface wheel or rail provides relative displacement acts as input excitation to the system and corresponding excitation frequency is generated. In the present work it is assumed that wheel defects does not exist and overall track irregularities are the main source of excitation which is characterized and expressed by the PSD [25]. PSD measures the power per unit frequency to understand its distribution. PSD of track is related to the Fourier transform and auto correlation function of stochastic data. The PSD standards such as FRA, ORE (German standard), SIMPACK (DB), Anderson Characteristics, SNCF (France), The Braun (ISO), Chinese and Indian railroad PSD standards etc. are commonly used for response analysis in their respective countries [2, 28]. An Indian Railroad PSD standard is used for modelling and response analysis of LHB coach in present work.

2.2.1. Indian rail road PSD

The vertical and lateral PSD of track irregularities for Indian Rail road is obtained from the work of Iyengar and Jaiswal [29]. The origin of which can be traced to Research and Design Standards Organization (RDSO) Lucknow, Government of India, Ministry of Indian Railway. It can be expressed as $S(\Omega) = C_{sp}\ \Omega^{-N}$ [2].Where, C_{sp} is an empirical constant and 'N' characterizes the rate at which amplitude decreases with frequency. The variation of auto correlation PSD terms of vertical and lateral unevenness are given as a function of spatial frequency Ω at corresponding wheel-rail contact point using,

$$S_v(\Omega) = 0.0958\,\Omega^{-2.1382} \quad (1)$$

$$S_a(\Omega) = 0.0554\,\Omega^{-2.2686} \quad (2)$$

The unit of this spatial frequency Ω is mm^2/cycle/m [11-12]. The 'Ω' is related to the exciting cyclic frequency (f) Hz as $f = \Omega \times v = \frac{1}{\lambda} \times v$, where v = speed of vehicle and λ is the wavelength of track irregularity. For cross correlation PSD terms, auto correlation terms are multiplied by $e^{i\omega t}$. In the unit of PSD cycle/m represents spatial frequency with respect to wavelength (λ) that can be denoted by Ω by its units of m^{-1}. Therefore, unit of PSD is converted and made compatible while conducting response analysis using $S_v(f) = \frac{S_v(\Omega) \text{ or } S_a(\Omega)}{v}$.

2.3. Modelling of LHB coach of rail vehicle

German design 2 tier wider cabin typical LHB rail passenger coach broad gauge (BG) type subjected to 4 DOF and running at constant an average speed PSD of 90 km/h on irregular track of long wavelength (λ) is considered for response analysis. The 4 DOF includes bounce, lateral, roll and pitch motions. In general as shown in Fig. 2, LHB coach consists many suspended mechanical and electrical equipments underneath coach body for passenger amenity, braking and lighting needs which can play substantial role in its dynamic behaviour and comfort level of passengers. The vital mechanical and electrical equipments such as pneumatic brake panel, under slung tanks, bio toilet tanks, battery box and transformer unit are considered in the dynamic analysis.

The side and end views of physical model are shown in Fig. 3. The modelling assumptions are as follows,

1) Coach body and bogie frame section is assumed as an Euler beam.
2) Each wheel axle set is running as single wheel and total load is supported by 4 wheels.
3) Bolster's mass at ends is assumed as an additional lumped mass at connectivity points.
4) Rail track is treated rigid structure and right and left rail surfaces have same irregularities.
5) Each node on model is subjected to 4 DOF while nodes at the wheel axles are subjected to 2 DOF.
6) All suspended equipments are assumed to be concentrically located along the coach body axis.
7) Creep forces at contact point are ignored and only linear contact spring is considered.

Only long wavelength irregularities in the range of 0.5-250 m are considered for the modelling. The coach is modelled using FE method.

2.3.1. Mathematical model

The direct FEM approach is used for node connectivity and model the coach body and bogie frame. It is divided into number of elements and nodes in which each node represents a point of concern for response analysis. The axes of a single element model like discretized beam element in space subjected to 3 translational and 3 rotational DOF as shown in Fig. 4 [30]. Fig. 5 represents a single element under 4 DOF motions in which the elemental mass matrix [Me] and stiffness matrix [Ke] can be derived from Eqns. (3) to (6).

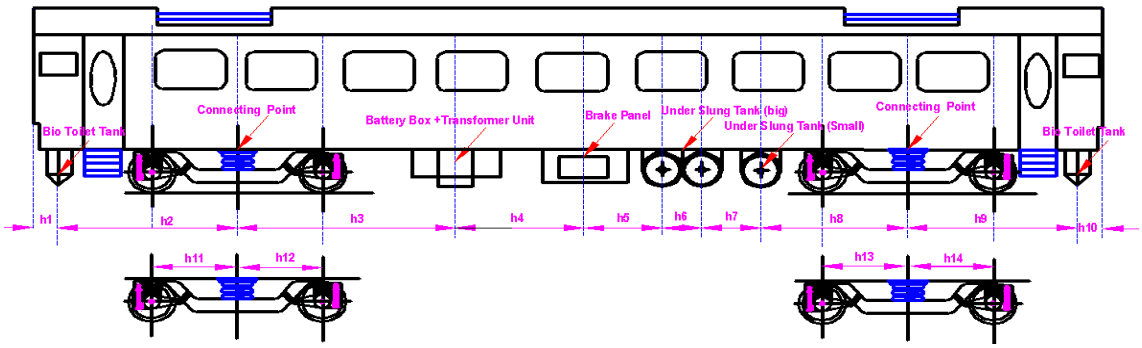

Fig. 2: LHB coach lay out

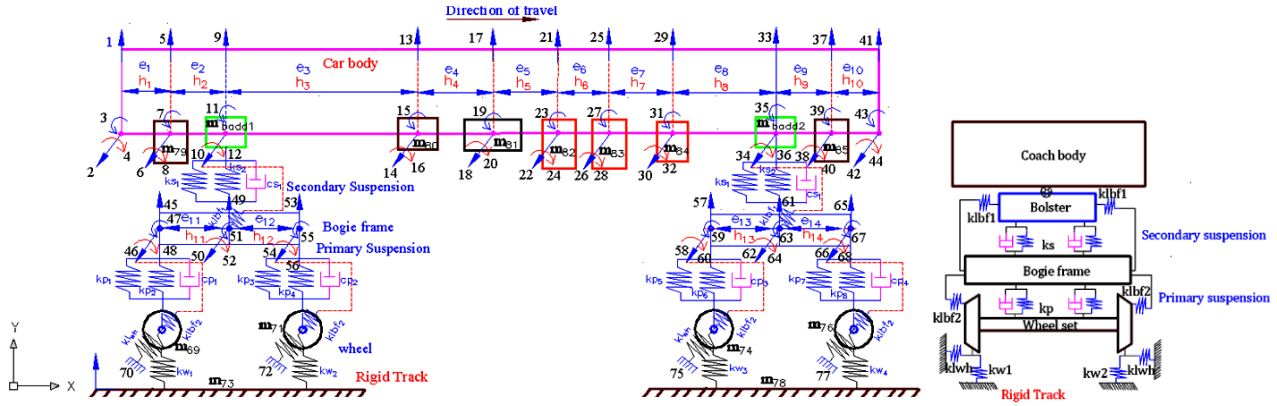

Fig. 3: Physical LHB coach model, Side view (Left) and End view (right)

$$[M_e] = \frac{\rho A h}{420}$$

	d_1x	d_1y	d_1z	ϕ_1x	ϕ_1y	ϕ_1z	d_2x	d_2y	d_2z	ϕ_2x	ϕ_2y	ϕ_2z
d_1x	140	0	0	0	0	0	70	0	0	0	0	0
d_1y	0	156	0	0	0	22h	0	54	0	0	0	-13h
d_1z	0	0	156	0	-22h	0	0	0	54	0	13h	0
ϕ_1x	0	0	0	$140rg^2$	0	0	0	0	-13h	0	$-3h^2$	0
ϕ_1y	0	0	-22h	0	$4h^2$	0	-13h	0	0	0	$-3h^2$	0
ϕ_1z	0	22h	0	0	0	$4h^2$	0	13h	0	0	0	$-3h^2$
d_2x	70	0	0	0	-13h	0	140	0	0	0	0	0
d_2y	0	54	0	0	0	13h	0	156	0	0	0	-22h
d_2z	0	0	54	-13h	0	0	0	0	156	0	22h	0
ϕ_2x	0	0	0	0	0	0	0	0	0	$140rg^2$	0	0
ϕ_2y	0	0	13h	$-3h^2$	$-3h^2$	0	0	0	22h	0	$4h^2$	0
ϕ_2z	0	-13h	0	0	0	$-3h^2$	0	-22h	0	0	0	$4h^2$

(3)

$$[K_e] = \begin{array}{c|cccccccccccc} & d_1x & d_1y & d_1z & \phi_1x & \phi_1y & \phi_1z & d_2x & d_2y & d_2z & \phi_2x & \phi_2y & \phi_2z \\ d_1x & \frac{AE}{h} & 0 & 0 & 0 & 0 & 0 & -\frac{AE}{h} & 0 & 0 & 0 & 0 & 0 \\ d_1y & 0 & \frac{12EI_z}{h^3} & 0 & 0 & 0 & \frac{6EI_z}{h^2} & 0 & -\frac{12EI_z}{h^3} & 0 & 0 & 0 & \frac{6EI_z}{h^2} \\ d_1z & 0 & 0 & \frac{12EI_y}{h^3} & 0 & -\frac{6EI_y}{h^2} & 0 & 0 & 0 & -\frac{12EI_y}{h^3} & 0 & -\frac{6EI_y}{h^2} & 0 \\ \phi_1x & 0 & 0 & 0 & \frac{GJ}{h} & 0 & 0 & 0 & 0 & 0 & -\frac{GJ}{h} & 0 & 0 \\ \phi_1y & 0 & 0 & -\frac{6EI_y}{h^2} & 0 & \frac{4EI_y}{h} & 0 & 0 & 0 & \frac{6EI_y}{h^2} & 0 & \frac{2EI_y}{h} & 0 \\ \phi_1z & 0 & \frac{6EI_z}{h^2} & 0 & 0 & 0 & \frac{4EI_z}{h} & 0 & -\frac{6EI_z}{h^2} & 0 & 0 & 0 & \frac{2EI_z}{h} \\ d_2x & -\frac{AE}{h} & 0 & 0 & 0 & 0 & 0 & \frac{AE}{h} & 0 & 0 & 0 & 0 & 0 \\ d_2y & 0 & -\frac{12EI_z}{h^3} & 0 & 0 & 0 & -\frac{6EI_z}{h^2} & 0 & \frac{12EI_z}{h^3} & 0 & 0 & 0 & -\frac{6EI_z}{h^2} \\ d_2z & 0 & 0 & -\frac{12EI_y}{h^3} & 0 & \frac{6EI_y}{h^2} & 0 & 0 & 0 & \frac{12EI_y}{h^3} & 0 & \frac{6EI_y}{h^2} & 0 \\ \phi_2x & 0 & 0 & 0 & -\frac{GJ}{h} & 0 & 0 & 0 & 0 & 0 & \frac{GJ}{h} & 0 & 0 \\ \phi_2y & 0 & 0 & -\frac{6EI_y}{h^2} & 0 & \frac{2EI_y}{h} & 0 & 0 & 0 & \frac{6EI_y}{h^2} & 0 & \frac{4EI_y}{h} & 0 \\ \phi_2z & 0 & \frac{6EI_z}{h^2} & 0 & 0 & 0 & \frac{2EI_z}{h} & 0 & -\frac{6EI_z}{h^2} & 0 & 0 & 0 & \frac{4EI_z}{h} \end{array} \quad (4)$$

$$[M_e] = \frac{\rho A}{420}$$

$$\begin{array}{c|cccccccc} & d_1y & d_1z & \phi_1x & \phi_1z & d_2y & d_2z & \phi_2x & \phi_2z \\ d_1y & 156h & 0 & 0 & 22h^2 & 54h & 0 & 0 & -13h^2 \\ d_1z & 0 & 156h & 0 & 0 & 0 & 54h & 0 & 0 \\ \phi_1x & 0 & 0 & 140rg^2 & 0 & 0 & -13h^2 & 0 & 0 \\ \phi_1z & 22h^2 & 0 & 0 & 4h^3 & 13h^2 & 0 & 0 & -3h^3 \\ d_2y & 54h & 0 & 0 & 13h^2 & 156h & 0 & 0 & -22h^2 \\ d_2z & 0 & 54h & -13h^2 & 0 & 0 & 156h & 0 & 0 \\ \phi_2x & 0 & 0 & 0 & 0 & 0 & 0 & 140rg^2 & 0 \\ \phi_2z & -13h^2 & 0 & 0 & -3h^3 & -22h^2 & 0 & 0 & 4h^3 \end{array} \quad (5)$$

$$[K_e] = \begin{array}{c|cccccccc} & d_1y & d_1z & \phi_1x & \phi_1z & d_2y & d_2z & \phi_2x & \phi_2z \\ d_1y & \frac{12EI_z}{h^3} & 0 & 0 & \frac{6EI_z}{h^2} & -\frac{12EI_z}{h^3} & 0 & 0 & \frac{6EI_z}{h^2} \\ d_1z & 0 & \frac{12EI_y}{h^3} & 0 & 0 & 0 & -\frac{12EI_y}{h^3} & 0 & 0 \\ \phi_1x & 0 & 0 & \frac{GJ}{h} & 0 & 0 & 0 & -\frac{GJ}{h} & 0 \\ \phi_1z & \frac{6EI_z}{h^2} & 0 & 0 & \frac{4EI_z}{h} & -\frac{6EI_z}{h^2} & 0 & 0 & \frac{2EI_z}{h} \\ d_2y & -\frac{12EI_z}{h^3} & 0 & 0 & -\frac{6EI_z}{h^2} & \frac{12EI_z}{h^3} & 0 & 0 & -\frac{6EI_z}{h^2} \\ d_2z & 0 & -\frac{12EI_y}{h^3} & 0 & 0 & 0 & \frac{12EI_y}{h^3} & 0 & 0 \\ \phi_2x & 0 & 0 & -\frac{GJ}{h} & 0 & 0 & 0 & \frac{GJ}{h} & 0 \\ \phi_2z & \frac{6EI_z}{h^2} & 0 & 0 & \frac{2EI_z}{h} & -\frac{6EI_z}{h^2} & 0 & 0 & \frac{4EI_z}{h} \end{array} \quad (6)$$

Table 1: Relative spatial distances of under frame suspended equipment

Description of suspended equipment	Distances	Values
Distance between left free end and center of bio-digester tank	h_1	1.39m
Distance between center of bio toilet tank and bogie connectivity of coach body	h_2	2.93 m
Distance between center of bogie connectivity of coach body and of (T/U+B/Box)	h_3	6.92 m
Distance between center of (T/U +B/Box) and brake panel	h_4	1.48 m
Distance between center of brake panel and 1st big under slung tank	h_5	1.42 m
Distance between center of 1st and 2nd big under slung tank	h_6	0.85 m
Distance between center of 2nd big and small under slung tank	h_7	1.65 m
Distance between center of small under slung tank (UST) and bogie connectivity of coach body	h_8	2.58 m
Distance between center of bogie connectivity and of bio toilet tank	h_9	2.93 m
Distance between center of bio toilet tank and right free end of coach body	h_{10}	1.39 m
Distance between left free end and center of both bogies frame	$h_{11} = h_{13}$	1.28 m
Distance between right free end and center of both bogies frame	$h_{12} = h_{14}$	1.28 m

Key nomenclatures are: ρ = Mass density of frame material, r_g = radius of gyration = J/A, J= Polar cross sectional moment of inertia, I_z and I_y are the cross sectional moment of inertia about z-z and y-y axis respectively, E = Modulus of elasticity of frame structure and h's = Nodal distance. The dimensions of spatial distances ($h_1 \ldots h_{14}$) of suspended equipment are taken from RCF, Kapurthala drawing for equipments and given in Table 1. The mass of coach body in loaded condition is taken as 30639.2 kg. Taking $\rho_1 = 7740 kg/m^3$ for coach body material, volume and area of cross section calculated as $3.95m^3$ and $0.167m^2$ respectively. Refer Table 3 and Fig. 6, taking b_i and d_i as 3120 mm and 2935 mm, existing values of A_1 ($b_o \times d_o - b_i \times d_i$ = 0.870 m^2) is not equal to $0.167m^2$. It is because of hollow wall section. So, its existing cross sectional area is required to be transformed into new assumed cross sectional area that comes to be equal to 0.167 m^2. In new assumed cross section, the outer dimensions are to be retained as it is and variation is given in inner dimensions to maintain effect of sectional MI of coach body. The new values of di' and bi' determined as 3050 mm and 3233 mm and therefore, the relation of $b_0 d_0 - b_i' d_i' = 0.167$ is satisfied. The I_{z1} sectional MI (about z-z axis) and I_{y1} (about y-y axis) are calculated using,

$$I_{z1} = \frac{1}{12}[b_o(d_o)^3 - b_i'(d_i')^3 = 0.3608m^4 \quad (7)$$

$$I_{y1} = \frac{1}{12}[d_o(b_o)^3 - d_i'(b_i')^3 = 0.1835m^4 \quad (8)$$

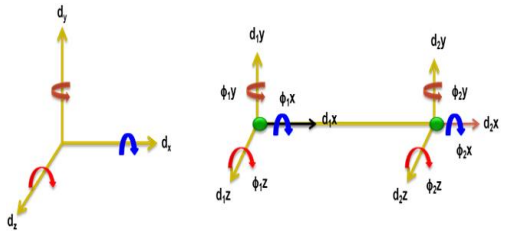

Fig. 4: Beam subject to 3 translational and 3 rotational motions

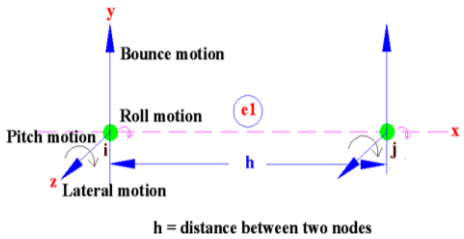

Fig. 5: Degrees of freedom in element considered for modelling

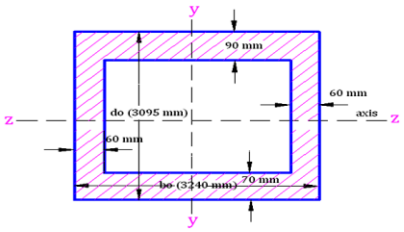

Fig. 6: Cross section of coach body

The data for FIAT bogie frame as shown in Fig.7 is calculated. Referring to Fig. 8, plane of bogie frame cross section lies on y-z plane. Taking ρ_2 = 7806kg/m^3 and data from Tables 1 & 3, area of cross section and its MI about z-z axis are calculated using,

$$I_{z2} = 2 \times (I_{GG} + A_2 \times y^2) = 2 \times \left[\frac{1}{12}\left[b_o {d_o}^3 - b_i {d_i}^3\right] + (b_o d_o - b_i d_i) \times y^2\right] = 3.0 \times 10^{-3} m^4 \quad (9)$$

Where, $y = \frac{419}{2} + \frac{290}{2} = 354.5$ mm, vertical distance from z-z axis to the centres of section and is taken from Rail Coach Factory Kapurthala (Punjab), India - drawing for bogie frame.

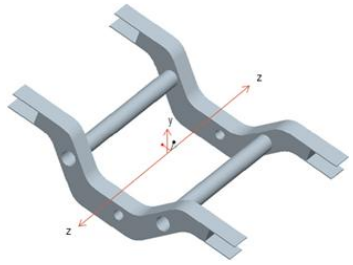

Fig. 7: FIAT bogie frame

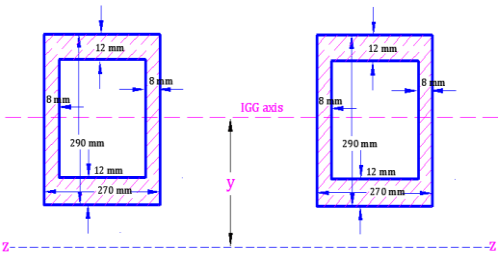

Fig. 8: FIAT bogie frame cross section about z-z axis

Refer to Fig. 9, the sectional MI about y-y is calculated using,

$$Iy_2 = I_{GG} + A \times z^2 = 2 \times \left[\frac{1}{12}\left[d_o {b_o}^3 - d_i {b_i}^3\right] + (b_o d_o - b_i d_i) \times z^2\right] = 0.0305 \text{ m}^4 \quad (10)$$

Where z = 2240/2 = 1120mm, vertical distance from y-y axis to the centres of the section as taken from Rail Coach Factory Kapurthala (Punjab), India - drawing for bogie frame. The values other parametric data such as masses, lengths, modulus of elasticity and rigidity, wire and coil diameters of springs and its equivalent stiffness are given in Tables 2 to 6 [11,31]. The suspension stiffness is calculated using $k = Gd^4/(8D^3n)$.

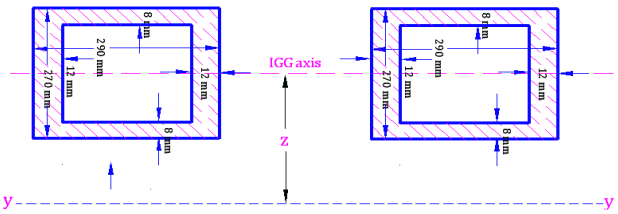

Fig. 9: FIAT bogie frame cross section about y-y axis

Table 2: Coach mass data

Description	Mass
Gross Mass of coach (tare) of coach	46720kg
Mass of bogie frame	2600kg
Tare mass of coach	41600kg
Mass of wheel set	1600kg
Mass of battery box	235kg
Mass of transformer unit	400kg
Mass of full tank of bio toilet tank	425kg
Mass of each bolster	400kg
Mass of each coupler jumper	231.4kg
Mass of each bogie	6300kg
Mass of brake panel	450kg
Mass of UST$_1$ (big) (fully loaded)	685+315 = 1000kg
Mass of UST$_2$ (big) (fully loaded)	685+315 = 1000kg
Mass of UST$_3$ (small) (fully loaded)	(143+450) = 593kg
Mass of each battery	26.12kg
Total no .of battery	9
Mass of bio toilet tank (E)	120kg
Nos. of bio toilet tank per coach	3

Table 3: Coach geometrical data

Description	Dimensions
Length over body	23540 mm
Width over body	3240 mm
Height over body	3095 mm
Distance between center pivots	14900 mm
Bogie length	3534 mm
Bogie width	3030 mm
Bogie frame plate thickness vertical	8 mm
Floor thickness	70 mm (approx.)
Side wall thickness	60 mm(approx.)
Roof thickness	90 mm(approx.)
Wheel base	2560 mm
Bogie frame height	290 mm
Bogie frame breadth	270 mm
Bogie frame plate thickness horizontal	12 mm

Table 4: Parameters used in global stiffness and mass matrix

Parameter	Coach body	Bogie frame	Generic
I_z (m^4)	0.3608	3.0×10^{-3}	
I_y (m^4)	0.1835	0.030	
A (m^2)	0.167	0.094	
ρ ($kg/m^{3)}$	7406	7806	
k_h (N/m)			1.11×10^9
E (N/m^2)			2.0×10^{11}
G (N/m^2)			79.3×10^9

In LHB coach, primary suspension consists inner and outer springs whereas secondary suspension includes inner, outer and rubber springs. Starting from left end wheel axle sets of rear bogie, outer, inner and middle spring's stiffness are calculated and given in Table 5. The stiffness of middle i.e. rubber spring is taken as 0.25×10^5 N/m [32]. Vertical and lateral wheel rail contact spring stiffness is denoted by k_w and k_{lwh}. The structural fitting between bolster and bogie frame is treated as lateral spring and its stiffness denoted by k_{lbf1}. Similarly, between bogie frame and wheel axles are denoted by k_{lbf2}. Bolster element rigidly connected with coach body, is assumed to act as integral part like additional lump masses at their corresponding connectivity points [31]. As shown in Fig. 3, coach model consists of 78 DOF in total and the rotational DOF are reduced using Guyan reduction technique [22]. The final model after reduction comes to be 38 DOF which contains vertical and lateral motions at global nodal points of the coach as shown in Fig. 10. The suspension data for the coach is given in Table 6. The Eqn. of motion for multi DOF can be expressed by,

$$[M]\{\ddot{x}\} + [C]\{\dot{x}\} + [K]\{x\} = \{F\} \quad (11)$$

Where, [M], [C] and [K] represent global mass, damping and stiffness matrices and {F} is external force input excitation vector. The Eqn. (11) is solved for its Eigen values solution where first 8 natural frequencies of the system are obtained as 0.41, 0.82, 0.91, 6.18, 6.18, 8.95, 8.95 and 12.48 Hz. The determination of damping matrix [C] and external force input excitation matrix [SF (ω)] follows in the next subsections.

Table 6: Coach Suspension data

Parameters	Primary Suspension		Secondary Suspension	
	Outer	Inner	Outer	Inner
Outer dia.(Do)	257 mm	164mm	418 mm	280+0/-2 mm
Inner dia.(Di)	181+3/-0 mm	112+3/-0 mm	318+3/-0 mm	212 mm
Mean dia.(D)	220.5 mm	139.5 mm	369.5 mm	246 mm
Wire dia. (d)	38 mm	26 mm	50mm	34 mm
Nos. of coils.(n)	5.5	7.5	6.6	8.3

Table 5: Equivalent suspension data

Primary, secondary suspensions, vertical, lateral wheels and bogie frame stiffness									
Outer	Values	Inner	Values	Outer	Values	Inner	Values	Middle	Values
kp_1	3.38×10^5N/m	kp_2	2.15×10^5N/m	ks_1	1.79×10^5N/m	k_{s2}	1.02×10^5N/m	k_{s3} (rubber)	0.25×10^5 N/m
kp_3	3.38×10^5N/m	k p_4	2.15×10^5N/m	ks_4	1.79×10^5N/m	k_{s5}	1.02×10^5N/m	k_{s6} (rubber)	0.25×10^5N/m
kp_5	3.38×10^5N/m	kp_6	2.15×10^5N/m	k_{w1}	0.55×10^8N/m	k_{w2}	0.55×10^8N/m	k_{w3}	0.55×10^8N/m
kp_7	3.38×10^5N/m	kp_8	2.15×10^5N/m	k_{w4}	0.55×10^8N/m	k_{lbf1}	0.2324MN/m	k_{lbf2}	11.5MN/m
*kpe_{12}	(kp1+kp2)×2=11.06×10^5N/m			k_{lwh}	250 MN/m	*kse_{13}	(ks1+ks2+ks3) × 2 = 6.12×10^5N/m		
*kpe_{34}	(kp3+kp4)×2=11.06×10^5N/m			*kse_{46}			(ks4+ks5+ks6) × 2=6.12×10^5N/m		
*kpe_{56}	(kp5+kp6)×2=11.06×10^5N/m			$kw_{e1}=kw_{e2}=kw_{e3}=kw_{e4}$			1.11×10^9N/m		
*kpe_{78}	(kp7+kp8)×2 =11.06×10^5 N/m			*Denotes equivalent spring stiffness of primary and secondary suspension. The kwe_1, kwe_2, kwe_3 and kwe_4 denote equivalent stiffness of corresponding wheel axles					

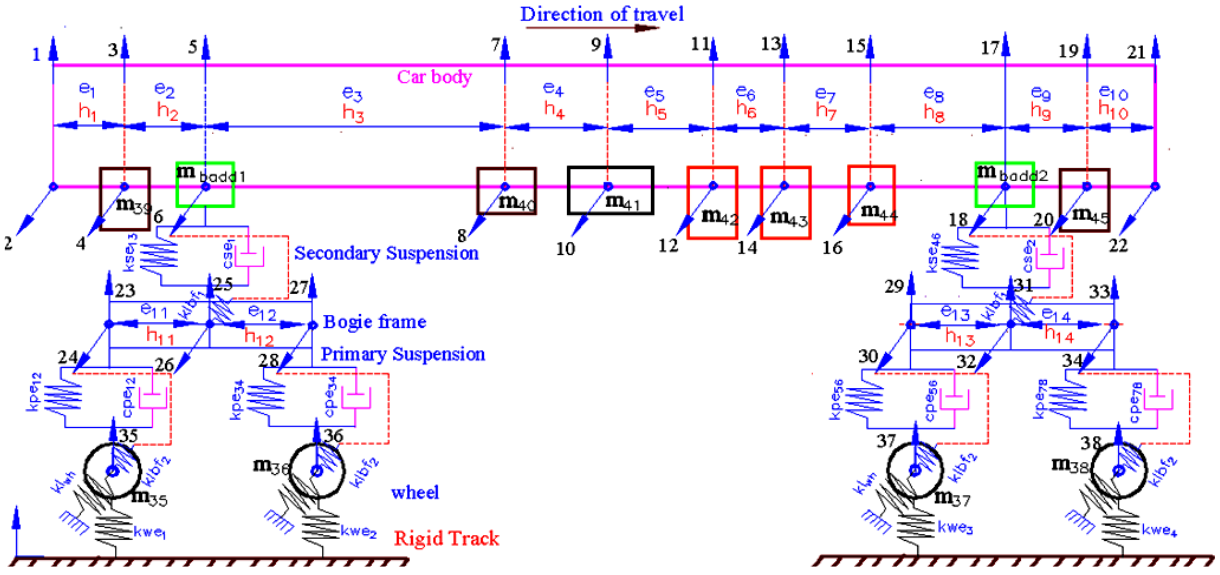

Fig. 10: Physical model of LHB coach showing 38 DOF after Guyan reduction

2.3.2. Determination of damping matrix [C]

For [C], the complete system is primarily considered under the effect of structural damping matrix [H] which is formed by taking 2.5 % of [K] (for low carbon steel or alloy) and diagonalized as H_Norm = $\phi^T H \phi$ with mass normalized eigenvector ϕ. The structural damping is converted into equivalent modal viscous damping coefficients using,

$$c_{eq} = (\alpha/\pi\omega) \quad (12)$$

Where, α = Structural damping coefficient and 'ω' is the natural frequency. A diagonal matrix [H_1] is formed in terms of $\pi_{\omega n}$ with n = 1, 2, 3…etc. The equivalent viscous damping matrix C_1 is formed by C_1 = H_Norm × $[H\_1]^{-1}$. Next, viscous damping coefficient matrix C_2 as per connectivity of actual dampers is formed and diagonalized as C_Norm = $\phi^T C_2 \phi$. The modal damping matrix 'C' is then determined from $C=C_1+C\_Norm$ as a diagonal matrix [.cr.]. Thus overall matrix [C] can be obtained from $\phi^T[C]\phi=[.cr.]$. Thus damping matrix [C] is given by,

$$[C] = \phi^{-T}\,[.cr.]\,\phi^{-1} = \phi\,[.cr.]\,\phi^T \quad (13)$$

The values of damping coefficient i.e. 32600 N-s/m and 40200 N-s/m of actual primary & secondary dampers used in matrix C_2 are taken from RCF, Kapurthala (Punjab), India - Drawing for dampers.

2.3.3. Input force excitation in terms of PSD

Younesian & Nankali [13] described that exciting force at wheel- rail contact point is equal to the product of square of linear hertz contact spring stiffness (k_h) and PSD of track. The same assertion was also made by Wei Gao et al for road car wheel contact surface randomness (x_r) i.e. distribution of irregularities [23, 33]. When this external force is applied with $x_r{}^2$, then it works as PSD from which input exciting force in terms of PSD (S_0) is given by,

$$F_{ext} = k_h{}^2 S_0 \quad (14)$$

The value of k_h is obtained from wheel rail contact model as shown in Fig. 11. The wheel rail contact force is defined by non-linear Hertz contact theory using [4-5],

$$F = C_H \times y^{\frac{3}{2}} \quad (15)$$

Where C_H [N m$^{-3/2}$] is a constant depending on the radii and material properties of wheel and rail and 'y' is depth of contact surface. Since frequency domain solution requires all components to be linear [14]. Therefore, linearized stiffness 'k_h' is derived as [4],

$$k_h = \frac{dF}{dy} = \frac{3}{2}\left(C_H{}^{2/3} F^{1/3}\right) {}^{N}/_{m} \quad (16)$$

The value of C_H is taken as 1.0 ×10^{11} and F = static load of LHB coach is 40600 kg and hence 'k_h' is calculated as 5.5×10^8 N/m per wheel.

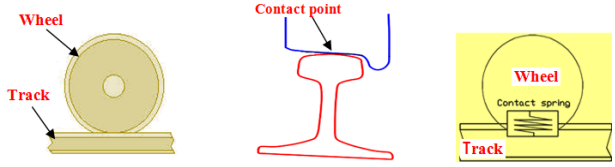

Fig. 11: Wheel rail contact spring

2.3.4. Input force spectral density matrix [34]

The input loading PSD force matrix SF_{ij} (ω) can be formed by Fourier transform of load vector P (t). While forming this it is assumed that axle is running on the same rail profiles with one wheel lags the other such that $x_2(t) = x_1(t)$, then cross spectral density is expressed by,

$$SF_{12}(\omega) = S_0 e^{-i\omega t} \text{ and } SF_{21}(\omega) = S_0 e^{i\omega t} \quad (17)$$

Where, S_0 is the spectral density matrix function of auto correlation and't' is the time lag, such that t = l/v where 'l' denotes wheel axle spacing and 'v' train speed. The complete spectral density matrix for 4 wheels axles can be given by,

$$SF(\omega)_{ij} = \begin{bmatrix} Si_1j_1(\omega) & Si_1j_2(\omega) & \dots & Si_1j_n(\omega) \\ Si_2j_1(\omega) & Si_2j_2(\omega) & \dots & Si_2j_n(\omega) \\ \dots & \dots & \dots & \dots \\ Si_nj_1(\omega) & Si_nj_2(\omega) & \dots & Si_nj_n(\omega) \end{bmatrix} \quad (18)$$

The diagonal terms S_{ii} (ω) is the auto correlation function of load P_i (t) and the off diagonal terms S_{ij} (ω) is the cross correlation function between load P_i (t) and P_j (t). Gangadharan et al [12] described that if the input from left rail is completely correlated with that of the right rail, then the system can be simplified to a case of four random loadings. Assuming that left and right track surfaces have the same irregularities and wheels are fully correlated at any instant, then running of wheels of an axle on two rails can be regarded as running of single wheel on single rail and thus the reduced coach model be running with 4 wheels on single rail in place of 8 wheels on track and the input force spectral matrix $[S_F(\omega)]_{38\times38}$ in terms of PSD is given by,

$$S_F(\omega)_{38\times38} = \begin{array}{c|cc} & 34 & 4 \\ \hline 34 & SF_{11}(\omega) & SF_{12}(\omega) \\ 4 & SF_{21}(\omega) & SF_{22}(\omega) \end{array} \quad (19)$$

Where, SF_{11} (ω), SF_{12} (ω), SF_{21} (ω) contains all elements zero and SF_{22} (ω) is given by 4×4 input force spectral matrix in terms of ($k_h{}^2$×S_0) in which diagonal elements represent auto correlation terms of SF_{11} (ω) = SF_{22} (ω) = SF_{33} (ω) = SF_{44} (ω) = ($k_h{}^2$×S_0) whereas off diagonal elements represent cross correlated terms. The complete 4×4 input force spectral density matrix is given by,

$$\begin{bmatrix} & 35 & 36 & 37 & 38 \\ 35 & SF_{11}(\omega) & SF_{12}(\omega) & SF_{13}(\omega) & SF_{14}(\omega) \\ 36 & SF_{21}(\omega) & SF_{22}(\omega) & SF_{23}(\omega) & SF_{24}(\omega) \\ 37 & SF_{31}(\omega) & SF_{32}(\omega) & SF_{33}(\omega) & SF_{34}(\omega) \\ 38 & SF_{41}(\omega) & SF_{42}(\omega) & SF_{43}(\omega) & SF_{44}(\omega) \end{bmatrix} \quad (20)$$

The off diagonal elements SF_{12} (ω), SF_{13} (ω), SF_{14} (ω), SF_{23} (ω), SF_{24} (ω) and SF_{34} (ω) are calculated with corresponding time lag of wheels arriving at same exciting points. Therefore, the terms of symmetrical matrix are calculated as SF_{12} (ω), = SF_{11} (ω) $e^{\omega\tau1}$, SF_{13} = SF_{11} (ω) $e^{\omega\tau2}$, SF_{14} = SF_{11} (ω) $e^{\omega\tau3}$, SF_{23} = SF_{11} (ω) $e^{\omega\tau4}$, SF_{24} (ω) = SF_{11} (ω) $e^{\omega\tau5}$ and SF_{34} = SF_{11} (ω) $e^{\omega\tau6}$ [2, 12]. The relative spatial distances among the 4 wheels represented by b_1…b_6 are shown in Fig. 12 and the corresponding time lag τ_1, τ_2, τ_3 and τ_4 amongst the wheels are calculated by b/v; where v, b and ω are the speed, wheels spacing and exciting frequency respectively. Table 7 represents various time lag and

spatial distances of $b_1 \ldots b_6$ for 90 km/h speed of coach run. The following section deals with the determination of MSAR of LHB coach.

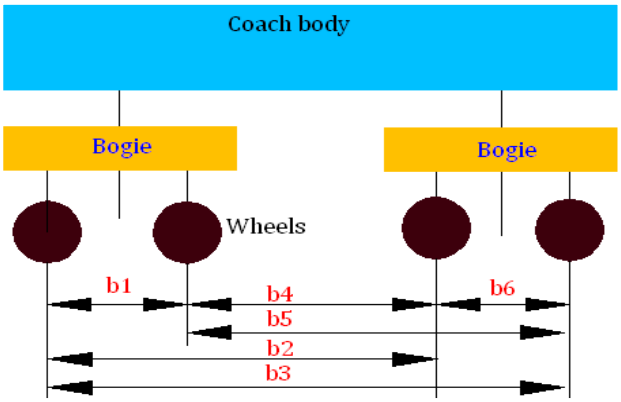

Fig. 12: Representation of auto and cross correlation of wheels

Table 7: Spatial distances of coach and time lag

Spatial distances	Values	Time lag	Values
b_1	2.56 m	τ_1	0.10 sec
b_2	14.9 m	τ_2	0.59 sec
b_3	17.46 m	τ_3	0.69 sec
b_4	12.34 m	τ_4	0.49 sec
b_5	14.9 m	τ_5	0.59 sec
b_6	2.56 m	τ_6	0.10 sec

2.4. MSAR analysis

For vertical and lateral track profile, a displacement PSD matrix of the model is obtained with the help of FRF or Transfer Function [6, 11, 13]. This FRF (H (ω)) in terms of natural and excitation frequency can be expressed by,

$$[H(\omega)] = \frac{1}{[(\omega_n{}^2 - \omega^2) + i\,(2\,\xi_n \omega\, \omega_n)]} \quad (21)$$

Where 'ω_n' and 'ω' are the natural and the exciting frequencies. The matrix [H (ω)] is a diagonal matrix in which k^{th} element can be represented by,

$$[H_k(\omega)] = \frac{1}{[(\omega_k{}^2 - \omega^2) + i\,(2\,\xi_k \omega\, \omega_k)]} \quad (22)$$

Where, $2\xi k$ is determined by,

$$2\,\xi_k \omega_k = C \quad (23)$$

Where, 'C' is a diagonalized modal damping matrix as calculated in Para. 2.3.2. and 'ω_k' and 'ω' are the k^{th} mode natural and exciting frequencies of the system. The displacement response PSD of car body is [6, 33],

$$[S_x(\omega)] = [\phi][H^*(\omega)][\phi]^T[S_F(\omega)][\phi][H(\omega)][\phi]^T \quad (24)$$

Where, $[\phi]_{38\times38}$, $[H(\omega)]_{38\times38}$ and $[H^*(\omega)]_{38\times38}$ are the normalized eigenvector matrix with mass matrix, diagonal FRF and its complex conjugate matrix. $[S_F(\omega)]$ is the input force spectral density function PSD matrix as given by Eqn. (19). From this, MSAR response of the system is given by the Eqn. (25) [11, 13, 16].

$$MSAR = (\omega)^4 \times S_x(\omega) = (2\pi f)^4 \times [\phi][H^*(\omega)][\phi]^T[S_F(\omega)][\phi][H(\omega)][\phi]^T \quad (25)$$

From the Eqns. (22), (24)-(25), plot of MSAR vs. exciting frequency in Hz is obtained considering excitation at front wheel of leading bogie for 0.1 - 40Hz frequency range of interest. The vertical and lateral response analysis is delineated in the next sections.

2.4.1. Vertical response at 90km/h constant speed

In reduced physical model as shown in Fig. 10, intuitively, it is assumed that there are five critical vertical DOF of the coach body namely 1, 3, 7, 19 and 21 which are at the locations of left free end, left end bio toilet tank 1, battery box + transformer unit, right end bio toilet tank 2 and right free end of coach body. The vertical acceleration PSD or response along these DOF is calculated using Eqns. (1) and (25) and given in Figs. 13(i)-(v) which represent vertical log acceleration response PSD in g^2/Hz and denoted by $\alpha_{1,38}$ - $\alpha_{21,38}$. Here, node 38 stands for leading wheel of front bogie. Results revealed that responses at various points of concern on coach body occur in low frequency (0-10Hz) range specifically at two consecutive frequencies namely at 0.91 and 6.18Hz etc. The peak responses at 0.91Hz are denoted by $\alpha_{1,38}$, $\alpha_{3,38}$ whereas other remaining three responses occurring at 6.18Hz are denoted by $\alpha_{7,38}$, $\alpha_{19,38}$, and $\alpha_{21,38}$. Peak responses occurring at low frequency range at constant speed PSD of vehicle run represents long wavelength irregularities of track which cause discomfort to the passengers. Since human sensitivity of comfort against vibratory motion falls in low frequency range (0.1-20 Hz) [35], so these responses are not desirable for comfort.

2.4.2. Lateral responses at 90 km/h constant speed

Refer to Fig. 10, the lateral responses are calculated at already discussed 05 critical points i.e. along 2, 4, 8, 20 and 22 DOF of the coach body using Eqns. (2) and (25) and given in Figs.14(i)-(v) which represent lateral log log acceleration response PSD in g^2/Hz and denoted by $\alpha_{2,38}$,-$\alpha_{22,38}$. Here, node 38 stands for leading wheel of front bogie. Results revealed that lateral responses at significant points on coach body also occur in low frequency (0-12.5 Hz) range specifically at 0.41 and, at around 12.5Hz frequencies. The first lateral peak response occurring at 0.41 Hz remains unchanged at various important junctions on coach body. This shows that lateral discomfort is perceived at comparatively longer wavelength irregularities of track which causes again discomfort to the passengers. These responses are not desirable and sound for comfort. However, another peak with lower magnitude occurs at some higher frequencies at around 12.5Hz which indicates smaller wavelength irregularities of track. Thus the overall occurrence of peak responses is observed within low frequency range (0-12.5Hz) which is still within susceptible frequency range to human being.

2.4.3 .Variation of vertical responses at various points of concern on coach body

Fig. 15 represents variation of peak responses at various points of concern on coach body. The points 1 and 2, shows occurrence of peak responses at frequency of 0.91 Hz whereas 3, 4 and 5 indicates at frequency 6.18 Hz. Thus all these variations occur in low frequency range (0-10Hz) and susceptible to human being. If excitation takes place at leading wheel of front bogie then magnitudes of responses at corresponding end of coach body is maximum whereas minimum occurs close to center point (3) i.e. location of battery box + transformer unit. However, response at left free end is observed to be greater than right free end.

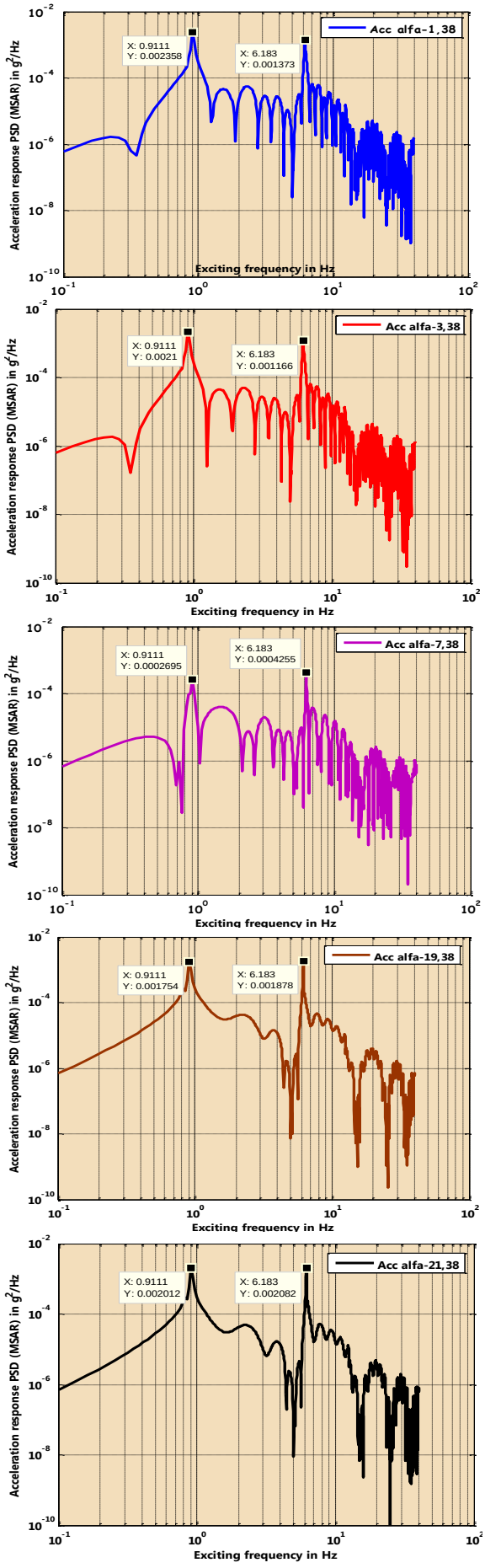

Fig. 13: Vertical responses at various locations on coach body

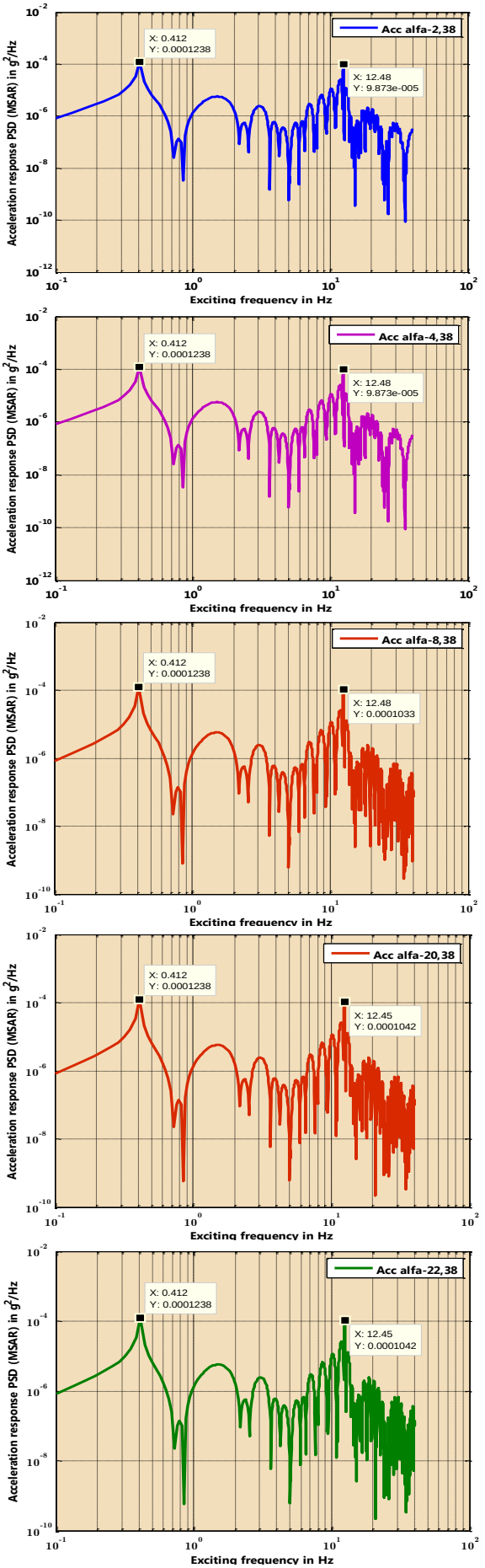

Fig. 14: Lateral responses at right free end of coach body

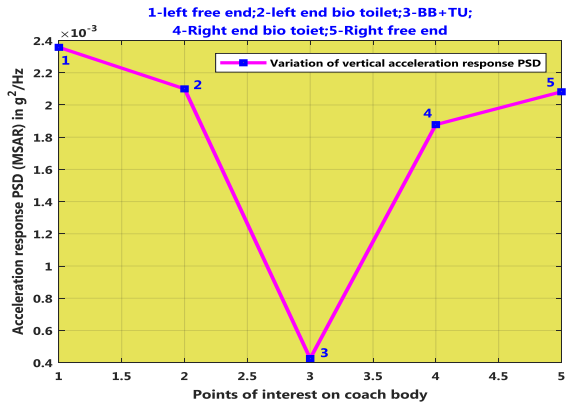

Fig. 15: Variation of relative vertical peak responses at various points of concern on coach body

2.4.4. Variation of lateral responses at various points of concern on coach body

The points 1, 2, 3, 4 and 5 in the Fig. 16 represents corresponding DOF of 2,4, 8,20 and 22 on coach body. The variation of peak responses at two consecutive frequencies is also shown.

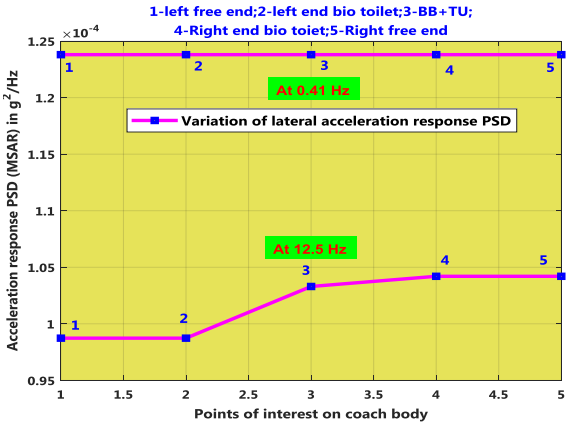

Fig. 16: Variation of relative lateral responses at various points of concern on coach body

2.5. Validation of results

Variation of MSAR as shown in Fig. 15 represents minimum response at vicinity to centre of coach body whereas the opposite ends have maximum. This depicts result validation and criteria that response level always accompanies with lower magnitude at center mass of coach body [10, 16]. Therefore, most of the researchers undertook response analysis at centre mass of coach body [11-12, 14]. To validate modelling result of present work, the MSAR level is compared with similar research work of literature [12]. Figs. 17 (a) and (b) represent linear plot for variation in vertical and lateral responses of present work at constant speed PSD of 90 km/h. Fig. 18 (a) and (b) denotes similar plot given by literature [12]. From Figs. 17(a) and 18(a), it is observed that vertical responses of present work is found to be in same order i.e. 10^{-4} g^2/Hz as by literature [12] but with slight differences in occurrence of peak response frequencies. However, the magnitudes of vertical peak responses of present work are observed to be around 1.5 times lower than literature [12]. Similarly from Figs. 17(b) and 18(b), it is observed that magnitudes of lateral peak responses in present work are found to be around 50 times lower than literature [12].

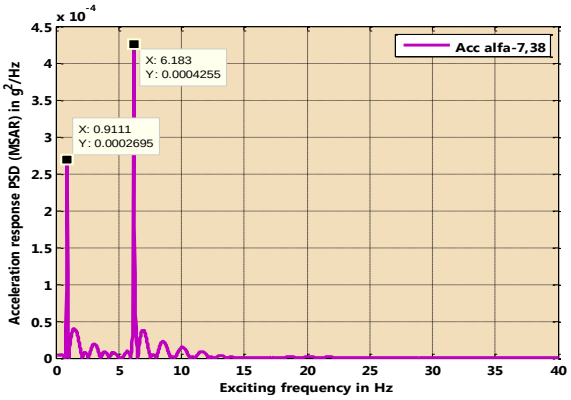

Fig. 17(a): Vertical responses

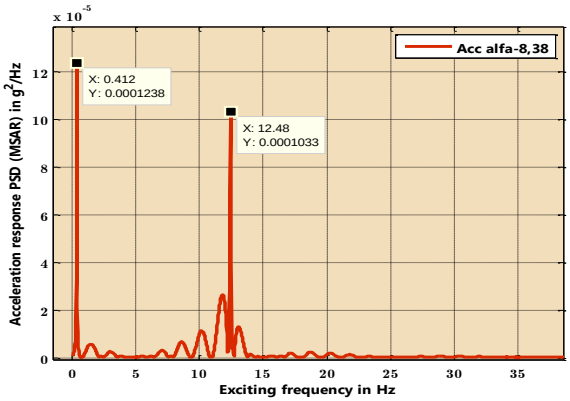

Fig. 17(b): Lateral responses

Fig. 17: Linear plots of acceleration response PSD at 90km/h constant speed run [Present work]

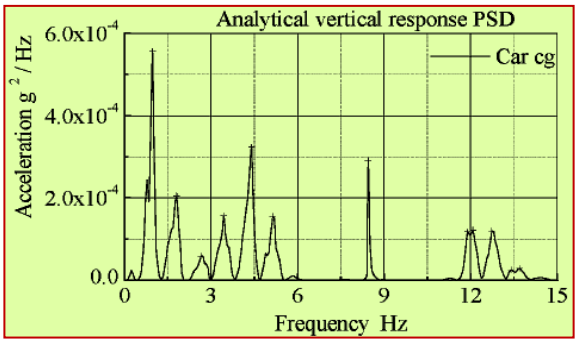

Fig. 18 (a): Vertical responses

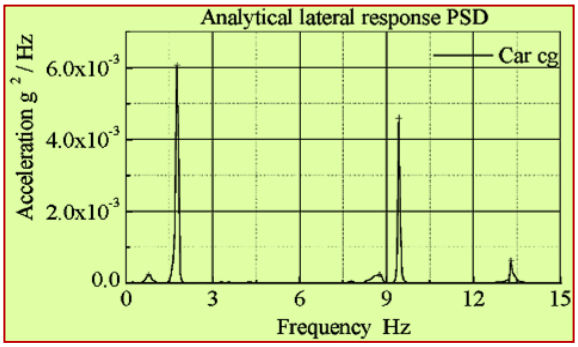

Fig. 18 (b): Lateral responses

Fig. 18: Linear plots of acceleration response PSD at 45km/h constant speed run [12]

3. Sensitivity analysis

Acceleration response PSD is dependent on FRF displacement or transfer function which is, moreover a

function of [K], [M] and [C] which further dependent on design parameters. These are the various relative equipment spacing (hs'), (h_w), (kpe_{12}, kpe_{34}, kpe_{56} and kpe_{78}) and (kse_{13} and kse_{46}), (kwe_1, kwe_2, kwe_3 and kwe_4) and (klw_h), $klbf_1$, and $klbf_2$, m_{39}, - m_{45} and damping coefficient of dampers etc. Each variable can affect response level either individually or simultaneously along with other parameters. In general, screening approach under 'Design of experiment (DOE)' is used to screen out most influential parameters in such situation. However, in present work instead of applying DOE, a mathematical approach for sensitivity analysis through partial derivative against FRF displacement of the system is performed. As it has been concluded that centre point of coach body has minimum response level, so centre mass of coach body is undertaken for study. Moreover, as vertical mode excitation is responsible for vertical and lateral responses and therefore sensitivity analysis is conducted on the basis of vertical response only. FRF displacement of a system can be expressed by,

$$\alpha(\omega) = \frac{1}{K-\omega^2 M+i\omega C} \quad (26)$$

Sensitivity analysis is conducted to check proneness of parameters against response. Damping in a system is to lower down amplitude of vibration and does not cast any effect on structural properties. Therefore, if the 'C' term in Eqn. (26) is removed then it does not affect sensitivity of the system and then FRF displacement in terms of [K] and [M] can be given by,

$$\alpha(\omega) = \frac{1}{K-\omega^2 M} \quad (27)$$

To find out an individual effect or sensitivity of variable, the partial derivative of FRF displacement α(ω) with respect to any variable 'p' is given by [36],

$$\frac{\partial \alpha(\omega)}{\partial p} = -(K-\omega^2 M)^{-1} \frac{\partial}{\partial p}(K-\omega^2 M)$$
$$= -\alpha(\omega)\left[\frac{\partial K}{\partial p} - \omega^2 \frac{\partial M}{\partial p}\right]\alpha(\omega) \quad (28)$$

In present analysis, the variables forming matrices [K] and [M] are of 3 categories i.e. relative spatial distances, stiffness and masses of suspended equipment. The partial derivatives of FRF displacement α (ω_r) with respect to variables h_r', k_r' and m_r' are expressed by,

$$\frac{\partial \alpha(\omega_r)}{\partial h_r} = -\alpha(\omega_r)\left[\frac{\partial K}{\partial h_r} - {\omega_r}^2 \frac{\partial M}{\partial h_r}\right]\alpha(\omega_r) \quad (29)$$

$$\frac{\partial \alpha(\omega_r)}{\partial k_r} = -\alpha(\omega_r)\left[\frac{\partial K}{\partial k_r} - {\omega_r}^2 \frac{\partial M}{\partial k_r}\right]\alpha(\omega_r) \quad (30)$$

$$\frac{\partial \alpha(\omega_r)}{\partial m_r} = -\alpha(\omega_r)\left[\frac{\partial K}{\partial m_r} - {\omega_r}^2 \frac{\partial M}{\partial m_r}\right]\alpha(\omega_r) \quad (31)$$

Where, $\omega_r = r^{th}$ Mode natural frequency; $m_r = r^{th}$ value of mass 'm' and $h_r = rt^h$ value of distance 'h' and K and M are reduced stiffness and mass matrix.

$\frac{\partial K}{\partial m_r}, \frac{\partial K}{\partial k_r}, \frac{\partial K}{\partial h_r}, \frac{\partial M}{\partial m_r}, \frac{\partial M}{\partial k_r}$ and $\frac{\partial M}{\partial h_r}$ in matrices expressed as

$$\frac{\partial K}{\partial m_r} = \begin{bmatrix} \frac{\partial K_{11}}{\partial m_r} & \frac{\partial K_{12}}{\partial m_r} \\ \frac{\partial K_{21}}{\partial m_r} & \frac{\partial K_{22}}{\partial m_r} \end{bmatrix}; \frac{\partial M}{\partial m_r} = \begin{bmatrix} \frac{\partial M_{11}}{\partial m_r} & \frac{\partial M_{12}}{\partial m_r} \\ \frac{\partial M_{21}}{\partial m_r} & \frac{\partial M_{22}}{\partial m_r} \end{bmatrix};$$

$$\frac{\partial K}{\partial k_r} = \begin{bmatrix} \frac{\partial K_{11}}{\partial k_r} & \frac{\partial K_{12}}{\partial k_r} \\ \frac{\partial K_{21}}{\partial k_r} & \frac{\partial K_{22}}{\partial k_r} \end{bmatrix}; \frac{\partial M}{\partial k_r} = \begin{bmatrix} \frac{\partial M_{11}}{\partial k_r} & \frac{\partial M_{12}}{\partial k_r} \\ \frac{\partial M_{21}}{\partial k_r} & \frac{\partial M_{22}}{\partial k_r} \end{bmatrix};$$

$$\frac{\partial K}{\partial h_r} = \begin{bmatrix} \frac{\partial K_{11}}{\partial h_r} & \frac{\partial K_{12}}{\partial h_r} \\ \frac{\partial K_{21}}{\partial h_r} & \frac{\partial K_{22}}{\partial h_r} \end{bmatrix}; \frac{\partial M}{\partial h_r} = \begin{bmatrix} \frac{\partial M_{11}}{\partial h_r} & \frac{\partial M_{12}}{\partial h_r} \\ \frac{\partial M_{21}}{\partial h_r} & \frac{\partial M_{22}}{\partial h_r} \end{bmatrix}$$

Since matrix [K] and [M] are not independent matrices but contains its sub matrices with retained and rotational DOF components. Therefore, Guyan reduction technique is used to obtain derivatives of matrices where reduced stiffness [K^R] and mass [M^R] matrices are expressed as,

$$[K^R] = EI[(K_{11}) - \{(K_{12})(K_{22})^{-1}(K_{21})\}] \quad (32)$$

$$[M^R] = \frac{\rho A}{420}[(M_{11}) - \{(M_{12})(M_{22})^{-1}(M_{21})\}] \quad (33)$$

$$[M^R] = \frac{\rho A}{420}[(M_{11})] \quad (34)$$

As translational mass DOF contains maximum energy level whereas rotational mass DOF with low energy level and hence the effect of latter is negligible than former retained DOF. Thus, the term $\{(M_{12})(M_{22})^{-1}(M_{21})\}$ in Eqn. (33) is ignored and Eqn. (34) is taken into account. A partial derivative of [K^R] with respect to h_1 is determined as below,

$$\frac{\partial}{\partial h_1}[K^R] =$$
$$EI\left[\frac{\partial}{\partial h_1}(K_{11}) - \left\{\left[\frac{\partial}{\partial h_1}(K_{12})\right](K_{22})^{-1}(K_{21}) + (K_{12})\left(\frac{\partial}{\partial h_1}[(K_{22})^{-1}]\right)(K_{21}) + (K_{12})(K_{22})^{-1}\left[\frac{\partial}{\partial h_1}(K_{21})\right]\right\}\right]$$
$$\text{for II}^{nd}\text{ term} =$$
$$(K_{12})\left[-(K_{22})^{-1}\left\{\frac{\partial}{\partial h_1}(K_{22})\right\}(K_{22})^{-1}\right](K_{21})$$

3.1. Sensitivity analysis with respect to relative spatial and wheel base distances

Using Eqn. (29) derivatives of α(ω) with respect to various relative spatial distances are obtained. For easy approach to sensitivity analysis, it is assumed that rail coach vehicle running with variable speed up to 350km/h on track having 5m long wavelength irregularities with constant speed (90km/h) PSD. Indian railroad vertical PSD standard is used for analysis and plots are drawn with the help of Matlab program. It is observed from Fig. 19 that when excitation takes place at leading wheel of front bogie, then sensitivity of distances fall in the order of $h_3 > h_{13} = h_{14} > h_{11} = h_{12} > h_1 = h_2 = h_4 = h_5 = h_6 = h_7 = h_8 = h_9 = h_{10}$.

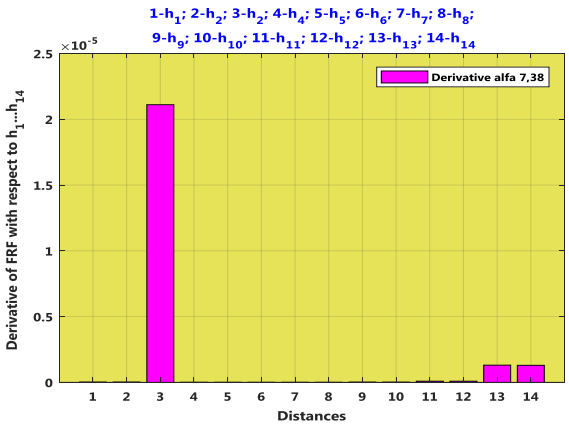

Fig. 19: FRF derivatives against distances when excitation at leading wheel of front bogie

Similarly, from the Fig. 20, when excitation takes place at trailing wheel of rear bogie, then sensitivity fall in the order of $h_3 > h_{11} = h_{12} > h_{13} = h_{14} > h_1 = h_2 = h_4 = h_5 = h_6 = h_7 = h_8 = h_9 = h_{10}$. It reveals us to conclude that 'h_3' is most sensitive against FRF displacement. Moreover, $h_{11} = h_{12}$ and $h_{13} = h_{14}$ are also equally sensitive against FRF displacement as the excitation point varies. Result concludes that 'h_3' is found to be one of the most sensitive parameter against response.

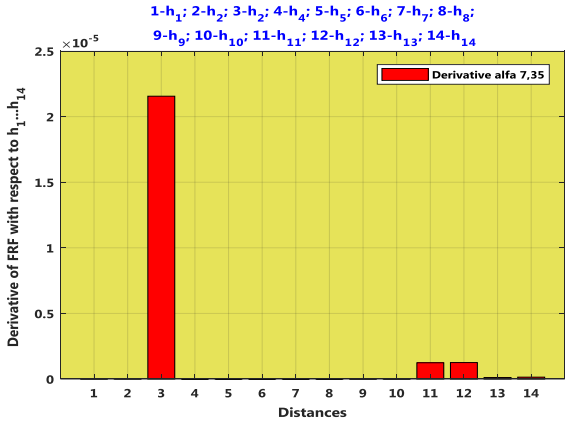

Fig. 20: FRF derivatives against distances when excitation at trailing wheel of rear bogie

3.2. Sensitivity analysis with respect to equivalent spring stiffness

Using Eqn. (30), derivatives of $\alpha(\omega)$ with respect to various stiffness are obtained.Where, k_r stands for stiffness's such as kpe_{12}, kpe_{34}, kpe_{56}, kpe_{78}, kse_{13}, and kse_{46} and wheel rail contact spring stiffness of kwe_1, kwe_2, kwe_3 and kwe_4 etc. The sensitivity analysis with respect to these parameters is carried out with the same values of wavelength, speed, PSD standard and constant PSD as given in Para.3.1. It is observed from the Fig. 21 that when excitation takes place at leading wheel of front bogie, then sensitivity of stiffness fall in the order of $kse_{46} > kpe_{56} = kpe_{78} > kse_{13} > kpe_{12} = kpe_{34} > kwe_1 = kwe_2 = kwe_3 = kwe_4$.

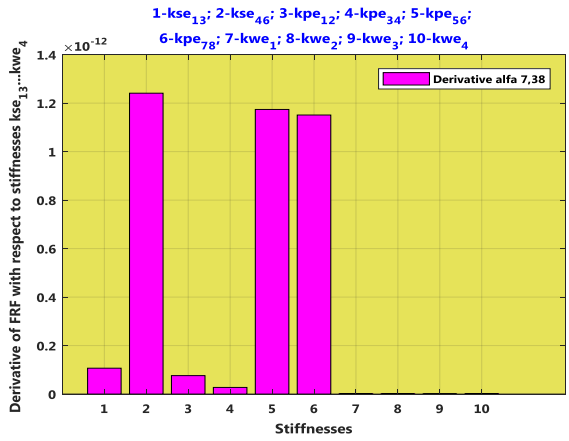

Fig. 21: FRF derivatives against stiffness when excitation at leading wheel of front bogie

Similarly, as shown in Fig. 22, when excitation takes place at trailing wheel of rear bogie, then sensitivity falls in the order of $kse_{13} > kpe_{34} > kpe_{12} > kpe_{78} > kse_{46} > kpe_{56} > kwe_1 = kwe_2 = kwe_3 = kwe_4$ with slightly lower magnitudes. This lends support to conclude us that kse_{46}, kse_{13}, kpe_{56}, kpe_{78}, kpe_{12} and kpe_{34} are equally most sensitive against FRF displacement as the point of excitation varies. Since $kpe_{56} = kpe_{78} = kpe_{12} = kpe_{34}$ and $kse_{46} = kse_{13}$, represent equivalent primary and secondary suspension stiffness, therefore, the equivalent primary and secondary suspension spring stiffness i.e. kpe_{12} and kse_{13} are found to be most sensitive parameter against response.

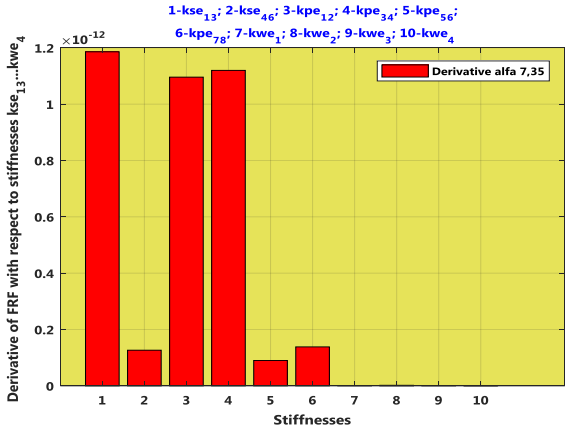

Fig. 22: FRF derivatives against stiffness when excitation at trailing wheel of rear bogie

3.3. Sensitivity analysis with respect to suspended equipment masses

Using Eqn. (31), derivative of $\alpha(\omega)$ with respect to various suspended equipment masses are obtained. Where, m_r stands for different masses and are denoted by m_{39}, m_{40}, m_{41}, m_{42}, m_{43}, m_{44} and m_{45}, and the sensitivity analysis with respect to these parameters is carried out with the same values of wavelength, speed, PSD standard and constant PSD as given in Para. 3.1. Fig. 23 and 24 represent FRF displacement derivatives with respect to various suspended masses when excitation takes place at leading wheel of front bogie and trailing wheel of rear bogie respectively. In both the cases m_{39} (mass of left end bio toilet tank) and m_{45} (mass of right end bio toilet tank) are found most influential parameters. However, m_{39} is observed to be as one the most sensitive parameter.

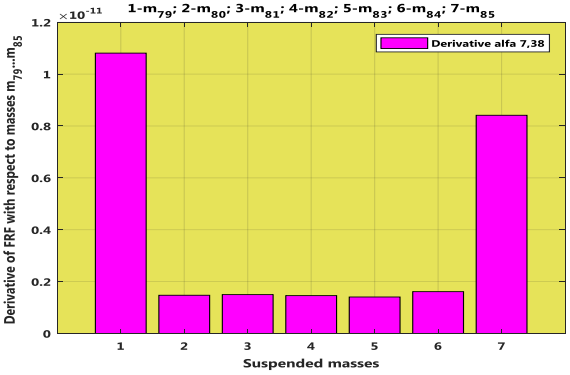

Fig. 23: FRF derivatives against masses when excitation at leading wheel of front bogie

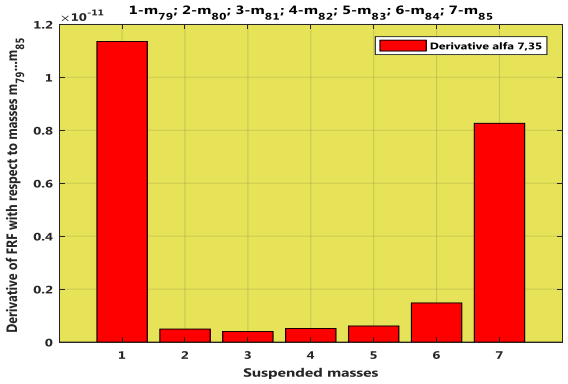

Fig. 24: FRF derivatives against masses when excitation at trailing wheel of rear bogie

4. Conclusion

This paper consolidates study of response analysis of an Indian Railway broad gauge designed AC 2 tier wider cabin LHB coach considering various suspended equipment with interaction of track PSD. The coach is modelled for 4 DOF coupled motions (bounce, lateral, roll & pitch) using FEM and reduced to those DOF which are of interest by Guyan reduction technique and Eigen solution obtained to determine the eigenvalues and eigenvectors. Vertical and lateral responses at close to centre mass of coach body are calculated and results validated with similar research work. The analysis has been carried out for 0.1- 40 Hz frequency range of interest with an average 90km/h constant speed PSD. Results indicate that vertical as well as lateral peak responses occur in low frequency range (0-12.5 Hz) which is not desirable for comfort as human being is susceptible in this frequency range**.**

This paper also addressed sensitivity analysis and has been observed that there are 4 parameters such as h_3 (relative spatial distance between left end connectivity of coach body with bogie frame and location of battery box + transformer unit), equivalent primary suspension stiffness k_{pe} (either one of kpe_{12}, kpe_{34}, kpe_{56} and kpe_{78}), equivalent secondary suspension stiffness k_{se} (either one of kse_{13} and kse_{46}) and m_{39} and m_{45} (masses of left and right end bio toilet tanks) found most sensitive design parameters of coach against FRF displacement. However, m_{39} is more sensitive than m_{45}. This suggests further scope for improvement in comfort level with minor adjustments of suspended equipment including suspension system of coach body without altering basic design of coach model. This study helps the rail coach designer and dynamists to improve the comfort levels of travel for the track PSD on optimizing these 4 most sensitive coach design parameters. These parameters may further be investigated for minimization of response by optimization through suitable optimization techniques.

ACKNOWLEDGEMENT:

This research work performed based on the physical AC 2 tier LHB designed coach model and its designed data. N. C. Railway Allahabad of Indian Railway has given permission to author to accomplish such research work while working as Senior Section Engineer of rail vehicle under C&W of Mechanical Engineering Department.

REFERENCES:

[1] S.R. Chandmal. 2013. Sensitivity analysis of ride behaviour of Indian railway Rajdhani coach using Lagrangian dynamics, *Int. J. Vehicle Structures & Systems*, 5(3), 84-89. http://dx.doi.org/10.4273/ijvss.5.3-4.02

[2] R.C. Sharma. 2011. Parametric analysis of rail vehicle parameters influencing ride behaviour, *Int. J. Engg., Sci. and Tech.*, 3(8), 54-65.

[3] D. Tore. 2004. Railway track settlements - A literature review, *Division of Solid Mechanics*, IKP, Linköping University, Sweden.

[4] Y.N. Sevgi, G. Rahmi, M. Muzaffer and Y. Hakan. 2007. Analyses of railway induced vibrations for different track types, *Inter-Noise*, Istanbul,Turkey.

[5] G. Bonin, G. Cantisani, M. Carbonari, G. Loprencipe and A. Pancotto. 2007. Railway traffic vibrations: generation and propagation - Theoretical aspects, *Proc. 4th Int. SIIV Congress*, Palermo, Italy.

[6] F. Cheli and R. Corradi. 2011. On rail vehicle vibrations induced by track unevenness: Analysis of the excitation mechanism, *J. Sound and Vibration*, 330, 3744-3765. https://doi.org/10.1016/j.jsv.2011.02.025.

[7] S. Mohammad zadeh, S.A. Mosayebi and R. Moosapoor. 2013. Investigating on the effects of random irregularities of railway track by half-bogie model, *Int. J. Advances in Railway Engg.*, 1(1), 61-75.

[8] W. Zhai and Z. Cai. 1991. Dynamic Interaction between a lumped mass vehicle and a discretely supported - continuous rail track, *Computers and Structures*, 63(5), 987-997. https://doi.org/10.1016/S0045-7949(96)00401-4.

[9] P. Broussinos and A.M. Kabe. 1991. *Multi-Mode Random Response Analysis Procedure*, Space System Division, Los Angeles, Air Force Base, EI Segundo, California.

[10] K.V. Gangadharan, C. Sujatha and V. Ramamurti. 2004. Experimental and analytical ride comfort evaluation of a railway coach, *Proc. IMAC-XXII A Conf. & Exposition on Structural Dynamics*, 249, Dearborn, Michigan, USA.

[11] R.C. Sharma. 2013. Modelling and simulation of railway vehicle system, *Int. J. Mech. Engg. and Robotics Research*, 1(1), 55-66.

[12] K.V. Gangadharan and C. Sujatha. 2008. Dynamic response of railroad vehicle: A frequency domain approach, *Int. J. Heavy Vehicle Systems*, 15(1), 65-81. https://doi.org/10.1504/IJHVS.2008.017984.

[13] D. Younesian and A. Nankali. 2009. Spectral optimization of suspension system of high speed trains, *Int. J. Vehicle Structure & System*, 1(4), 98-103. http://dx.doi.org/10.4273/ijvss.1.4.06.

[14] X. Jinhui, W. Biao, W. Li and W. Ping. 2016. Distribution characteristics and influencing factors of the frequency-domain response of a vehicle-track vertical coupled system, *J. Modern Transportation*, 24(3), 166-176. https://doi.org/10.1007/s40534-016-0111-9.

[15] R. Lupea and I. Curtean. 2012. A car component subjected to multiple sources of random vibrations, *Romanian J. Acoustics and Vibration*, 9(2), 117-122.

[16] D. Mădălina. 2013. Evaluation of the comfort index in railway vehicles depending on the vertical suspension features, *Annals of Faculty Engg. Hunedoara, Int. J. Engg.*, 23-32.

[17] W. Sun, D. Gong, J. Zhou and Y. Zhao. 2011. Influences of suspended equipment under car body on high speed train ride quality, *Proc. Engg., Int. Workshop on*

Automobile, Power and Energy Engg., 16, 812-817. https://doi.org/10.1016/j.proeng.2011.08.1159.

[18] B. Yulong, L. Yongle and D. Jiajie. 2016. A case study of dynamic response analysis and safety assessment for a suspended monorail system, *Int. J. Environmental Research and Public Health*, 13(11), 1121. https://doi.org/10.3390/ijerph13111121.

[19] R.C. Sharma. 2012. Recent advances in railway vehicle dynamics, *Int. J. Vehicle Structures & Systems*, 4(2), 52-63. http://dx.doi.org/10.4273/ijvss.4.2.04.

[20] W.M. To. 1990. *Sensitivity Analysis of Mechanical Structures Using Experimental Data*, Ph.D Thesis, Imperial College of Sci., Tech. And Medicine, University of London.

[21] D. Bhattacharjee, B. Malakar, P. Singh, S. Neog and B.K. Roy. 2016. Parametric sensitivity analysis of undercarriage components of a railway vehicle and their correlation to derailment safety and ride comfort, *Int. J. Control Theory and Applications*, 9(39), 83-94.

[22] R.J. Guyan. 1965. Reduced stiffness and mass matrices, *J. AIAA*, 3, 380. https://doi.org/10.2514/3.2874.

[23] W. Gao, N. Zhang and H.P. Du. 2007. A half car model for dynamic analysis of vehicles with random parameters, *Proc. 5th Australasian Congress on Applied Mechanics*.

[24] T. Dahlberg. 2006. *Track Issue*, Handbook of Railway vehicle dynamics, Taylor and Francis.

[25] J. Nielsen, E. Berggren, T. Lölgen, R. Müller, B. Stallaert and L. Pesqueux. 2013. Overview of methods for measurement of track irregularities important for ground-borne vibration, Deliverable D2.5, *Railway Induced Vibration Abatement Solutions*, Collaborative project.

[26] S.L. Grassie. 2009. Rail corrugation: characteristics, causes, and treatments, *Proc. IMechE Part F: J. Rail and Rapid Transit*, 223.

[27] C.J. Greisen. 2010. *Measurement, Simulation and Analysis of the Mechanical Response of Railroad Track*, University of Nebraska - Lincoln.

[28] G. Kouroussis, D.P. Connolly and O. Verlinden. 2014. Railway-induced ground vibrations - A review of vehicle effects, *Int. J. Rail Transportation*, 2(2), 69-110. https://doi.org/10.1080/23248378.2014.897791

[29] R.N. Iyengar and O.R. Jaiswal. 1995. Random field modeling of railway track irregularities, *J. Transportation Engg.*, 123(3), 303-308. https://doi.org/10.1061/(ASCE)0733-947X(1995)121: 4(303).

[30] C.S. Krishnamorthy. 2001. *Finite Element Analysis, Theory and Practice*, 2nd Ed., Tata Mc Graw-Hill Publication Co. Ltd., New Delhi.

[31] *Maintenance Manual for BG Coaches of LHB Design*. 2010. Research Design & Standards Organization, Ministry of Indian Railway, New Delhi.

[32] C.S. Woo, H.S. Park and D.C. Park. 2008. Evaluation of characteristics and useful life of rubber spring for railway vehicle, *Int. J. Railway*, 1(3), 122-127.

[33] W. Gao and N. Zhang. 2007. Dynamic analysis of vehicles with uncertain parameters, *Proc. 14th Int. Congress on Sound and Vibration*, Cairns, Australia.

[34] R.V. Field, T.L. Paez and D.O. Smallwood. 2007. *Validation of Random Vibration Environments*, Sandia National Laboratories, Albuquerque.

[35] R.C. Sharma. 2012. On the ride evaluation criteria of railway vehicles, *Indian Railway Technical Bulletin*, 5-9.

[36] D.J. Ewins. *Modal Testing: Theory, Practice and Application*, 2nd Ed., Research Studies Press Ltd., England.